WATER TUNNEL FORCE AND MOMENT STUDIES OF A MANEUVERING UCAV 1303 AND THEIR CONTROL

M.S. Chandrasekhara*, P.D. Sosebee, C.M. Medford*****
Naval Postgraduate School, Monterey CA 93943, USA
mchandra@nps.edu

Keywords: *UCAV unsteady aerodynamics, maneuver loads, unsteady flow control*

Abstract

The aerodynamic characteristics of a 1:72 scale, UCAV 1303 model were studied in a water tunnel using dye flow visualization and 5-component load balance. Data were obtained in both steady and unsteady flows at different Reynolds numbers for angles of attack from 0 to 30 deg and selected yaw angles. In unsteady flows, non-dimensional pitch rates of up to 0.1 were investigated for corresponding pitch and yaw angles. The results confirmed the previously reported tip-stall at low angles of attack and its adverse effects. Maneuver tests indicated dynamic lift was also produced on this aircraft. The maximum normal force value was 1.6 compared to the static case value of 0.8. Yawing the model produced strong side forces and rolling moments. Tip-stall and its effects were significantly mitigated when the leading edge radius over the full span was doubled. It did not alter the normal force behavior under unsteady conditions and promoted a smoother pitching moment. But the rapid moment rise occurred at a slightly lower angle of attack. The rolling moment increased measurably in all cases with increasing angle of attack. These results suggest that localizing the curvature change may hold some potential for further refinements of the observed characteristics.

1. Introduction:

Unmanned Combat Air Vehicles (UCAVs) have already proven effective in field applications in recent times. Their flow and aerodynamic characteristics have been studied by many [1-13] in steady flows. As these vehicles are called upon to perform defensive tasks during their operation, they will need to perform a range of maneuvers. Generally, a UCAV is designed to be tailless with a low radar cross section for low observability. This makes them unstable and most operate on the fringes of their narrow stability boundaries, placing a need for better performance [1]. Due to this limitation, the effects of cross winds and gusts are also important to their flight mechanics that are yet to be established. Also, being pilotless the current designs could benefit from dynamic stall phenomenon, if they can perform rapid aerodynamic maneuvers. However, due to their limited stability and thus, restricted operational envelope, such flight conditions are presently not conducive to this. Consequently, dynamic lift production has been simply avoided thus far, leaving out its benefits as well. It is also noted here that retention of dynamic lift thus produced also requires some flow control efforts.

In this study, the unsteady aerodynamic characteristics of a maneuvering UCAV 1303 were explored in the NPS water tunnel through flow visualization and a five-component strain gage load measurement balance studies. A USAF UCAV 1303 geometry that uses a non-slender, low leading edge sweep, cranked trailing edge delta wing with a blended wing/ fuselage was tested. It is known to produce unusual steady flow aerodynamic characteristics [2-7]. The most notable is the occurrence of tip-stall, at angles of attack as low as $\alpha = 2 - 4$ deg, over a wide range of Reynolds numbers and flow speeds. This causes normal force and pitching moment breaks in their respective distributions. Although the distributions recover at higher angles, since low angles of attack are normal for cruise conditions, it was felt worthwhile to investigate potential control means to mitigate the adverse effects of tip-stall.

Other unusual features include a distinctly different roll-up [2, 8, 10, 11, 14] of the well known slender delta wing type vortices. They roll-up from the back of the wing instead of all along it [14]; remain close to the surface and not way above it as slender wing vortices do. Even multiple, like-sense vortices can develop [14] depending upon the fuselage/wing junction flow. Both bubble and spiral vortex breakdown are present on the wing simultaneously [14]. It is also known [2, 8, 9, and 10] that the flow is extremely sensitive to leading edge surface features such as radius of curvature and roughness. This sensitivity may offer a potential flow control method and indeed, was exploited in this study.

dimensional rates; roll angle ϕ varying from 0-90 deg with the model held generally at fixed angles of attack studies at selected fixed positive yaw angles, ψ and dynamic pitch maneuvers for these. The paper builds on the results of [14] and discusses some key results pertaining to the aerodynamics of the vehicle; compares its performance in steady and unsteady flows and the effect of leading edge rounding [15] on the loads.

2. Description of the UCAV 1303 Model and Experiment

The UCAV 1303 geometry file was provided by the US Air Force from which two (nylon coated,

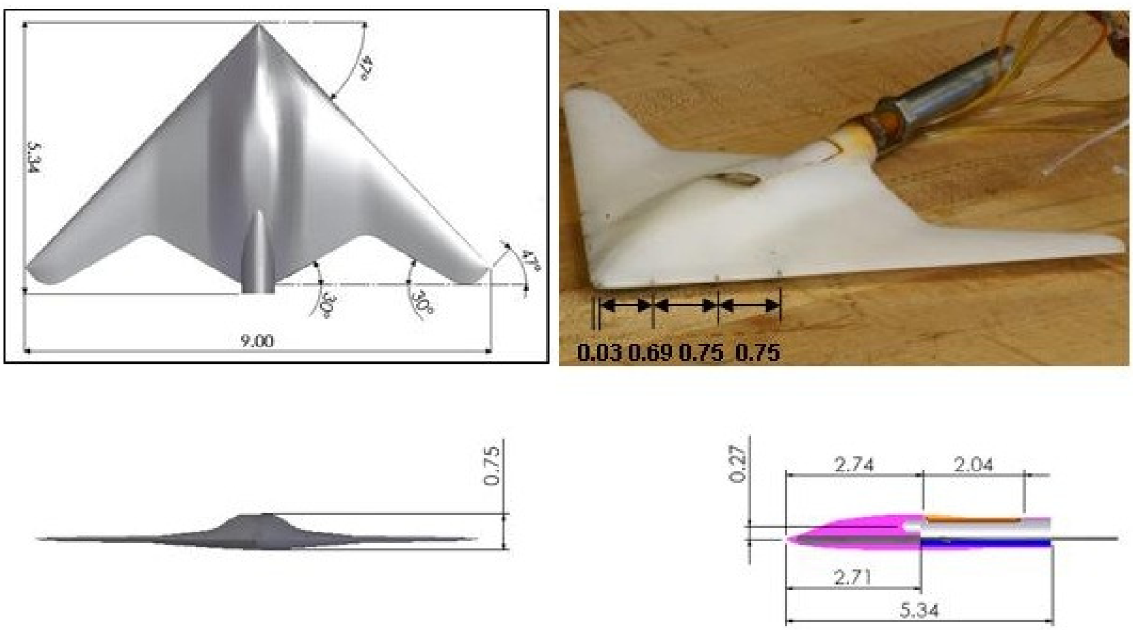

Fig. 1. UCAV 1303 model with dimensions (inches), and dye-ports (distances along the leading edge) as used in the NPS water tunnel

In further reviewing published literature, no data could be found on UCAV 1303 aerodynamic loading under yaw conditions in steady flows. This was also investigated briefly.

Furthermore, there is no flow field and load information available under unsteady flow conditions for the UCAV 1303 geometry. Hence, this became the emphasis for the present studies. Typical maneuvers studied included ramp-type pitch-up with angle of attack α varying from 0-30 deg at different non-

smooth) 1:72 scaled models, including the fuselage were built using rapid prototyping techniques; one for flow visualization and the other for load measurements. The actual model dimensions correspond to this scale ratio, with only the manufacturing process limitations affecting the final values when very small dimensions are concerned. Both NPS models were identical; the wing span was 9 in, root chord 5.34 in (with a nominally mean aerodynamic chord $\bar{c}$ of 3.54 in) and the fuselage 0.75 in thick respectively. The leading edge sweep was 47°; the trailing edge was cranked with sweeps of ± 30° and ± 47° as seen in Fig. 1. The leading edge radius was measured to be a constant 1/64 in. for most part due to the small scale (although the original configuration has a variation that is expected to be as shown in Fig. 2 of Wong, et al [6] who also made the model from the same geometry file).

The load model securely housed a water-proofed, five-component, internal strain gage balance with screws to an integral frame inside the model. It enabled measuring the normal force (N), side force (S), pitching moment (M), rolling moment (RM) and yawing moment (YM). The model was fabricated in two pieces with the first one accommodating the balance. The second piece was actually a portion of the original fuselage and was used to cover the balance and to maintain a smooth body exterior. The corresponding coefficients are defined in the usual manner and denoted as of C_N, Cs, C_M, C_{RM}, and C_{YM}.

Detailed load and moment measurements were conducted for steady and dynamic flow conditions. Typical dynamic motion consisted of rapidly pitching the model from 0 to 30 deg in a ramp-type maneuver, at different rates, even when the model was held at a specified yaw angle. For each unsteady experiment, loads and individual motion history were recorded. Ensemble averaging over typically 20 repetitive maneuvers (sometimes up to 100) was used in the data reported. The data were binned into narrow angle of attack range bins and the statistics were computed over the varying number of samples in each bin [13, 15].

For flow control experiments, a rounded leading edge radius of 1/32 in cast from fiber glass composite material to span the whole leading edge was taped to the wing surfaces. Details of this and related effort can be found in [15]. Other options were not considered in view of the low observability requirements.

2.1 Description of the Experiment

The NPS water tunnel (Rolling Hills Research Corp. RHRC Model 1520) was used for the experiments. Its dimensions are 15 in x 20 in x 60 in. Thus, blockage was not significant at all angles of attack. It is a free surface, open channel flow facility and hence the model is held upside down in order to eliminate any free surface effects during maneuvers. Thus, pitch-up here requires that the model nose tip be moved down. The model is held at its rear by a C-strut driven by a three-axis motion controller system, using stepper motors and gears, permitting any desired movement. Special care was taken during its design to eliminate differential motion between the C-strut and the model, which insured a one-one correspondence of the model motion with that of the strut. Both the water tunnel and C-strut are controlled by vendor supplied software.

Flow visualization studies were conducted using five dyes (red, green, yellow, blue and black) - food coloring diluted with water to be neutrally buoyant. The dye flow was carefully maintained at near zero momentum from each dye-port outlet on the model at all angles of attack. In this experiment, the same colored dye was supplied to corresponding outlets on the starboard and port sides of the model by using a splitter. Additionally and at times, black dye was injected externally from a tube which was used as a movable wand to explore flow details, such as wing tip-stall, or to verify if the underside flow rolled up when a vortex was produced, etc. Two Nikon digital D-80 cameras equipped with zoom lenses set up on tripods (one for starboard side flow views and the other at the bottom of the tunnel for plan views of the flow) were used for imaging. Flood lights illuminated the flow field. The camera shutters were remotely triggered simultaneously. For unsteady flow experiments custom developed LabVIEW based software and integrated hardware were used for phase locking purposes. The full details of the procedure can be found in Ref. [11, 12]. The unsteady flow experiments were conducted with a non-dimensional pitch rate defined as $\alpha^+ = \frac{\dot{\alpha}\bar{c}}{U_\infty}$, where $\dot{\alpha}$ is the pitch rate in radians/sec, $\bar{c}$ is the mean aerodynamic chord and U_∞ is the tunnel freestream velocity. In addition, dye-flow movies were obtained at different pitch rate (≈ 0.001 to 0.05) while the model pitched from 0 – 30 deg to dynamically record the flow evolution.

Both steady and unsteady flow load data were obtained in the body fixed coordinate system. The experiment was controlled by RHRC software. It was programmed to conduct tare tests for each case and generate a tare data file that was later used by their data processing software to calculate the actual loads and moments. In the unsteady maneuver studies, the data were ensemble averaged while the model executed specific maneuvers. Analysis of data acquired over as many as 100 runs led to the conclusion that ensemble averages over 20 repetitions were sufficient to yield stable aerodynamic coefficients. Data was collected over 40 sec, after a settling time of 15 sec for each maneuver. Typical maneuvers consisted of simple transient pitch-up at different rates and freestream speeds. This paper will restrict the results discussed to some steady flow visualization data at selected yaw angles at angles of attack and some dynamic loads. The effects of a rounded leading edge will also be reviewed.

2.3 Experiment Matrix

Results to be presented will focus on Re = 2.3 x 10^4, but the experiments were conducted for a wider range of conditions indicated below.

U_∞	6 in/sec	10 in/sec	14 in/sec
$Re_{\bar{c}}$	1.3 x 10^4	2. 3x 10^4	3.1 x 10^4
α^o	0 - 30	0 - 30	0 - 30
ψ^o	0, 2, 4, 6	0, 2, 4, 6	0, 2, 4, 6
$\Delta\alpha^o$	2	2	2
ϕ^o	0 - 90		
α^+	0.00, 0.05, 0.10, 0.15	0.00, 0.05, 0.10	0.00, 0.05

2.4 Experimental Uncertainties

It is pointed here that the loads measured in this study are very small because it is a low speed water tunnel, with small dynamic pressures even at its maximum speed – specifically less than 0.2 lbs. Thus, discrepancies can appear, especially at the lowest velocity of 6 in/sec, where in the maximum load was about 0.05 lb. With that consideration, the table of estimated experimental uncertainties is provided.

Parameter	% Uncertainty
U_∞	± 4 %
ρ	± 0.2 %
Normal Force	± 2 %
Side Force	± 0.5 %
Moments	± 1 %
C_N	± 5 %
C_M	± 3 %
C_S	± 1 %
C_{YM}	± 3 %
C_{RM}	± 3 %

Results and Discussion

3.1 Tip-stall and its modification

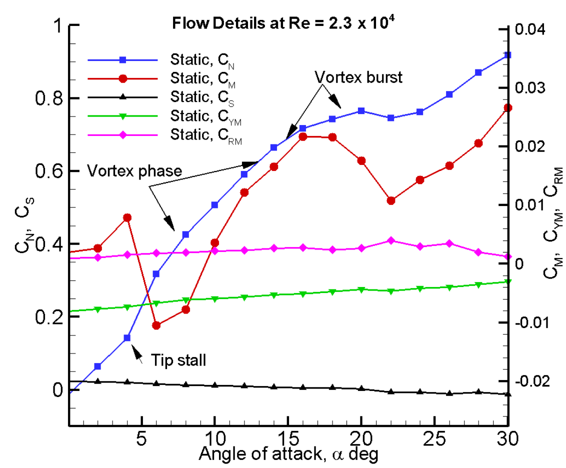

Fig. 2. Distributions of C_N, C_S, C_M, C_{YM}, and C_{RM} vs. α; $\alpha^+ = 0$, Re = 2.3 x 10^4, $\psi = 0$ deg.

The steady flow characteristics, in particular, the lift (or normal force) and pitching moment coefficient variation with angle of attack over a

UCAV 1303 can be found in several references [4-6]. Hence, these are only briefly discussed along with the new information of side force, rolling and yawing moment coefficients which are also presented in Fig. 2.

The most notable result seen in Fig. 2 is the generally smaller values of C_N with its maximum level of only about 0.8, prior to complete vortex bursting, which agree with others' values. It is also interesting that its variation with α is nonlinear, and there is a break at about α = 4 deg. This has been attributed to the occurrence of tip-stall based on detailed flow visualization studies [14] and is indicated in Fig. 2. The phenomenon arises from the breakdown of the vortices on both wings that are shed into the wake in the neighborhood of the trailing edge crank, upon which the flow spreads laterally outwards towards the wing tip, draws the surrounding fluid with it and eventually drives the tip flow upstream. The angle of attack and extent of tip-stall are somewhat dependent on Reynolds number, but the tendency is clear in most reported results, even at higher speeds and Reynolds numbers. The literature has focused more on the pitching moment development, wherein tip-stall appears more directly as a sharp pitch break, see red line in Fig. 2. Even though it is favorable around tip stall onset angle, the overall pitching moment distribution points to a tendency towards strong longitudinal instability until angles of attack around 16 deg; once again a common observation in the literature. At this angle, the vortices that form over the wing are in the process of breaking down. The breakdown mechanisms have been discussed by Gursul [8] and Chandrasekhara & McLain [14], amongst others. Corresponding variations can be seen in the side force, yawing moment and rolling moment coefficients. Since the UCAV 1303 is not equipped with a tail plane this would indicate a considerable need for a sizeable amount of control power to overcome the longitudinal instability problem. The side force, rolling moment and yawing moments also show small but discernible fluctuations around the tip stall angle, clearly establishing the need for incorporating sufficient control authority in the final design. This need also is apparent when the vortices burst, when the fluctuations are much larger as can be seen for angles of attack around 20-25 deg.

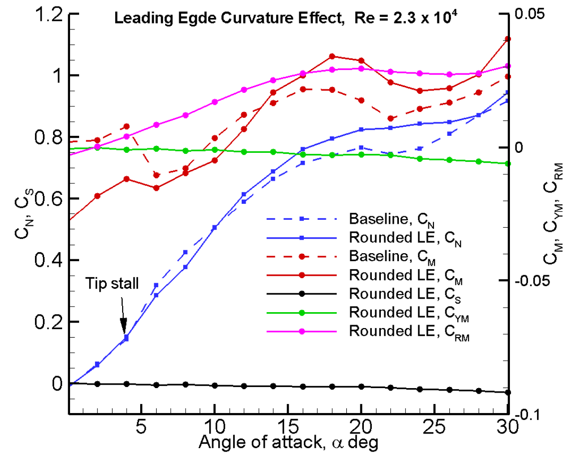

Fig. 3. Distributions of C_N, C_M, C_S, C_{YM}, & C_{RM} vs. α with rounded leading edge; $\alpha^+ = 0$, Re = 2.3×10^4, $\psi = 0$ deg

One goal of the present study was to alleviate tip-stall to the extent possible. As already mentioned, a rounded leading edge has been shown to offer some benefit in studies by McParlin et al [4] and could be also effective at the flow conditions studied here due to the response of the flow to wing leading edge curvature. The model was fitted with the rounded leading edge discussed in Sec. 2 and load data were collected for various Reynolds numbers. Fig. 3 presents these results. It is clear that the break in C_N (see Fig. 3a) discussed earlier is significantly reduced and the distributions look smoother for the increased leading edge curvature case (see solid lines). This benefit is obtained with a slight improvement of C_N as well. The corresponding C_M distribution is also softer around tip-stall angles of attack, and appears to be an improvement over the baseline case. It rises at a slightly lower α compared to the baseline case. No noteworthy changes can be seen in the C_S and C_{YM} data, although the C_{YM} values decrease with angle of attack for the rounded leading edge case. The most significant change is that the C_{RM} values seem to increase considerably over the angles studied. This same trend was observed for other Reynolds numbers at which the tests were conducted. This result leads one to conclude that further studies are needed to fully validate the concept deployed.

Primarily, the solution method used here was a simple glove like device over the entire leading edge from the apex to the wing tip. Since tip-stall is associated with the vortices emanating from near the trailing edge crank, it is quite possible that better success could result if only the portion of the leading edge that feeds the flow into this region is modified. Thus, a modification of the sectional leading edge curvature and its effects need to be investigated prior to adapting this approach to alleviate tip-stall without other significant effects.

3.2 Effects of yaw angle

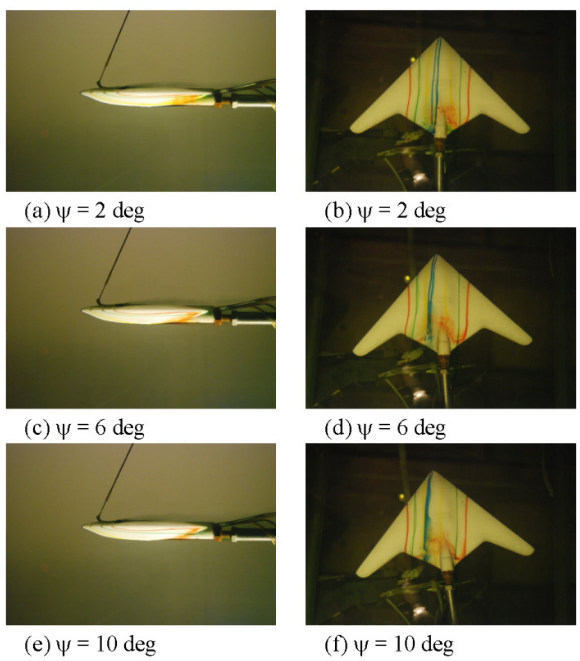

Fig. 4. Flow visualization images over a yawed UCAV 1303; Left: Side view, Right: Top view; Re = 3.1 x 10^4, α = 0 deg

The effects of yaw angle were studied in both steady and unsteady flow, for both the baseline airfoil and the rounded leading edge airfoil. Only specific yaw angles of 0, 2, 4, and 6 degrees were chosen for load studies, although up to 10 degrees of yaw were documented in flow visualization studies. The latter were limited to zero degree angle of attack. Fig. 4

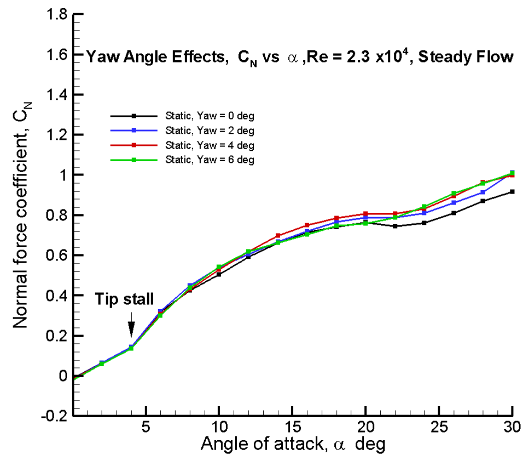

Fig. 5. Normal force coefficient distribution vs. angle of attack for different yaw angles; α^+ = 0, Re = 2.3 x 10^4

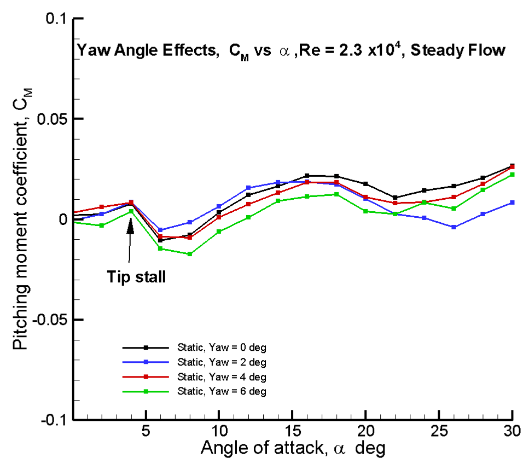

Fig. 6. Pitching moment coefficient distribution vs. angle of attack for different yaw angles; α^+ = 0, Re = 2.3 x 10^4

presents representative images (both starboard side and plan views) of the flow at Re = 3.1 x 10^4 and α = 0 deg, for the yaw angles shown with yawing to the port side. It is extremely interesting to see that the outboard (red) dye streaks have started to turn backwards between the trailing edge crank and engine even at zero angle of attack for low yaw angles. This is clearly seen in the side view pictures as well. It is contrary to intuitive reasoning that the flow turns toward the yaw direction which should relieve tip-stall on the opposite wing. The exact pattern was not as definitive at the lower Reynolds number cases studied, but still bore some resemblance to the above.

The effect of yaw on loads was also recorded and is shown in Fig. 5-7. Fig. 5 presents the normal force distributions, which indicate that for all yaw angles, despite local flow differences, tip-stall occurred at about the same angle of attack of 4 deg. Small differences appear in C_N only for larger angles of attack.

Likewise, the pitching moment coefficient shows some differences, but except for small offset values, exhibits relatively the same trend for all angles. These could be attributed to the flow differences as can be seen for the case of yaw = 6 deg, when the increase starts at slightly lower angles of attack.

Side force and yawing moment also showed similar behavior, with small differences. Fig. 7 shows the rolling moment coefficient for these cases and it changes from positive to negative values, more so with increasing yaw angle.

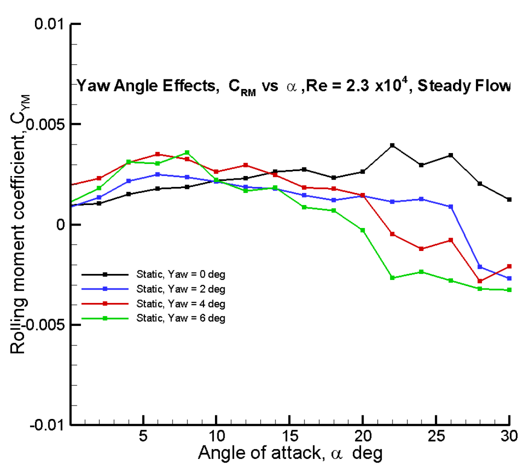

Fig. 7. Rolling moment coefficient distribution vs. angle of attack for different yaw angles; $\alpha^+ = 0$, Re = 2.3 x 10^4

3.3 Effects of Roll Angle

The model was held at different angles of attack and rolled from 0 to 90 deg towards the starboard side. Due to the model support mechanism used, it was not possible to generate

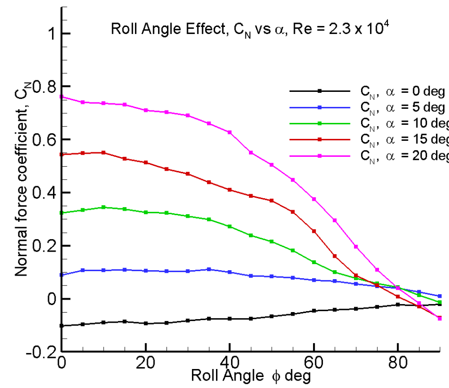

Normal force coefficient

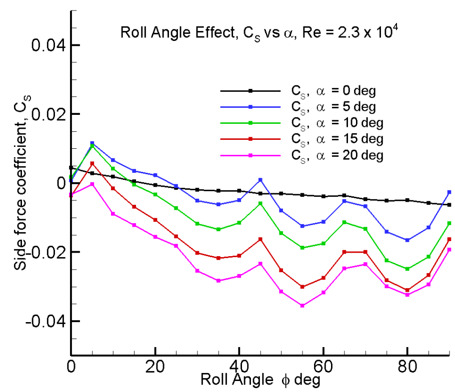

Side force coefficient

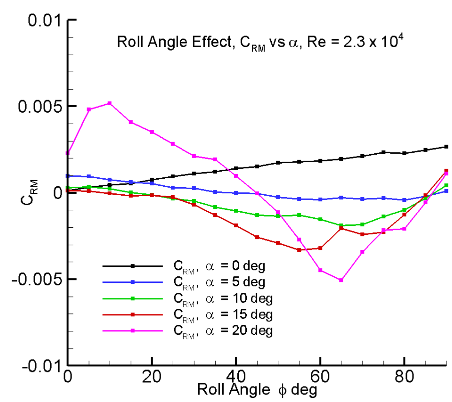

Rolling moment coefficient

Fig. 8. C_N, C_S, C_{RM} vs. roll angle for $\alpha^+ = 0$, Re = 1.3 x 10^4

a pure roll motion when it was at angles of attack and hence, additional angular movements were involved. In view of this, the data recorded is simply presented without giving any major interpretation.

The normal force, side force and rolling moment coefficients are shown in Fig. 8 (a-c). Basically, the normal force drops off to zero as the roll angle increases due to changes in the flow angles and thus, force components measured. The side force indicates vortical flow induced forces at different positions and the fluctuations observed suggest that there is some shedding activity accompanied by vortex re-formation that causes the variations. Rolling moment seems to be notably enhanced due to the orientation, especially at α = 20 deg when the initial vortex system has already begun to burst.

3.4 Effects of Unsteadiness

The model was pitched at two non-dimensional pitch rates α^+ (defined in Sec. 2.1) of 0.05 and 0.1 at the Reynolds numbers of the tests with a ramp type pitching history. Experiments were conducted also for pre-set yaw angles, for both the baseline airfoil and modified leading edge cases. Representative results will be presented and discussed.

Figure 9 shows that dynamically pitching the model from 0 to 30 deg has resulted in (1) elimination of tip-stall and resulted in a more linear normal force variation and (2) enhanced normal force values, particularly past the steady flow vortex bursting angles of attack. This is due to the production of dynamic lift by the rapid pitching motion. In 2-D dynamic stall flow, a vortex is produced and remains on the surface up to a higher (than static stall) angle of attack, which results in extra lift. For both pitch rates, similar increases are seen with the roll-off moving to slightly higher angles for the higher pitch rate case. This is a significant benefit, that if properly exploited could enable a superior maneuverability of the vehicle. A key point of interest here is that no new vortex is generated (as flow visualization images [14] have clearly demonstrated) because there is already a vortex on the wing that has formed earlier. So, it is believed that the dynamic pitching action only makes this vortex remain on the wing to a higher angle of attack (hence no jumps in C_N), by organizing the flow vorticity better. Chandrasekhara and McLain [14] discuss related issues more.

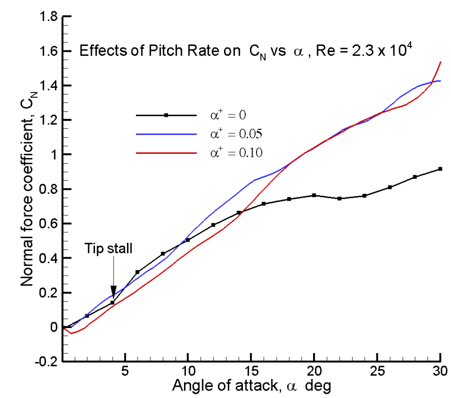

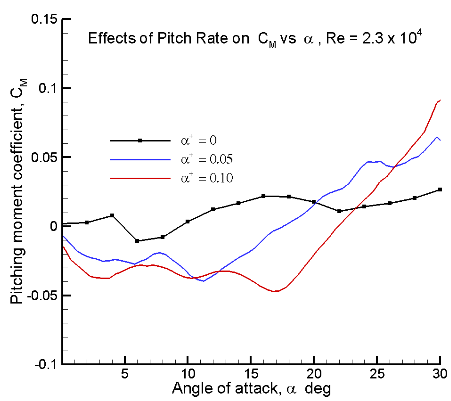

Fig. 9. Effect of pitch rate on C_N, C_M variation with angle of attack α; Re = 2.3 x 10^4

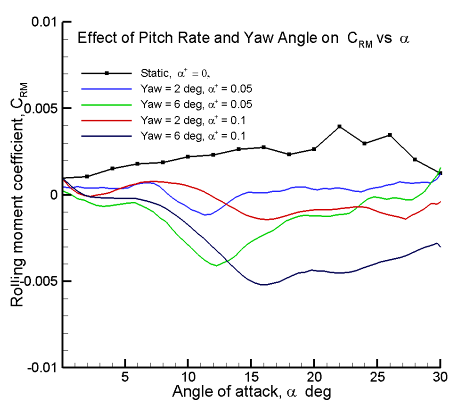

Fig. 10. Effect of unsteadiness on rolling moment coefficient C_{RM} variation with α; Re = 2.3 x 10^4

The above described flow, however, induces strong pitching moment variations, due to its eventual convection or bursting over the wing surface, which needs to be countered by the control system before satisfactorily exploiting this benefit. The concomitant pitching moment distributions shown at the bottom half of Fig. 9 confirm the larger and more unstable pitching moments produced. But, the rise occurs at a higher angle of attack for the higher pitch rate, indicating the delay in the onset of adverse pitching moment effects.

Regardless, it is clear that a rapid wing pitch-up places higher demands on the aircraft control systems. Interestingly, rapid pitching tends to organize the vorticity better on each wing, which reduces the side loads, rolling and yawing moments, although they show some oscillating characteristics.

When yaw is introduced with the pitch-up motion, essentially similar results are produced. However, because of the yaw, one can expect asymmetric vortical structure development, even with little change in the C_N behavior with α. This manifests as a change in the rolling moment, which depends on the pitch rate, as Fig. 10 demonstrates. The magnitude of C_{RM} increases with yaw angle, even in unsteady flows. The angle of attack where this peak occurs increases with pitch rate as well. A slight recovery and near level values are seen beyond the peak, indicating structural flow changes.

A rounded leading edge had little effect on the dynamic lift production. However, the pitching moment rise described in Fig. 9 occurred slightly earlier. The most notable result was the monotonically increasing rolling moment, akin to what was observed in steady flows. In the unsteady case, it continued to the highest angle of attack of the experiment.

4, Conclusions

The aerodynamic loads and moments over a maneuvering UCAV 1303 model were studied in the Naval Postgraduate School water tunnel at different Reynolds numbers and over an angle of attack range of 0 – 30 deg. Additionally, the effects of fixed yaw angles were investigated. A set of load data was also obtained by statically rolling the model through a 90 degree angle, when it was held at selected angles of attack. Attempts were made to control some undesirable flow features using leading edge curvature modification. The model was dynamically pitched at different rates. The NPS studies are the first such reported investigation. There is a reasonable body of lift and pitching moment data on the loads of the UCAV 1303 in the literature. However, the study being reported (and the earlier ones at NPS) also has measured 5 of the 6 force and moment components.

Occurrence of tip-stall is one of the major results reported earlier. It was verified here also. Tip-stall effects were mitigated by increasing the wing leading edge curvature from 1/64 in to 1/32 in. It caused the normal force distributions to became more linear, with little other changes. The pitching moment also became softer at the tip-stall angle of attack. However, the rise of pitching moment relative to the baseline case occurred at a slightly (by about 1-2 deg) lower angle of attack.

Studies with yaw angle varying showed an unexpected behavior of the flow turning towards the fuselage at zero angle of attack, regardless of the amount or direction of yaw. The C_{RM} values increased at larger yaw angles.

Roll angle produced asymmetry in the C_{RM} values, especially as the angle of attack was increased to 20 deg due to induced angles.

A near doubling of the maximum normal force coefficient to 1.6 was achieved by dynamically pitching the model, with small differences between non-dimensional pitch rates of 0.05 and 0.1 (higher C_N for the higher pitch rate case). No tip-stall was present in the dynamic pitching case. A rounded leading edge performed well, without any undue changes in the C_N behavior. The C_M behavior likewise was similar to the baseline case, with a slight advancing of the angle of attack of its rise. The rolling moment, however, showed an increase at higher angles of attack which needs to be addressed.

Further studies, wherein the leading edge curvature is only modified locally will need to be conducted prior to implementing this flow control approach at larger scales.

Acknowledgements

Funding for the project (TDSI/07-005/1A) was provided by the Singapore TDSI/Temasek Group under a CRADA with the US Naval Postgraduate School. The USAF provided the CAD geometry file. John Mobley of the MAE department provided shop and technical assistance throughout the program duration. Timely resolution of water tunnel issues was provided by Mike Kerho and Brian Kramer of Rolling Hills Research Corp., El Segundo, CA. All these are gratefully acknowledged.

References

[1] Cummings R.M. Morton S.A and Siegel S.G. Numerical prediction and wind tunnel experiment for a pitching unmanned combat air vehicle. *Aerospace Science and Technology J.* Dec. 2008, **12,** pp. 355-364.

[2] Ol M.V., "Water Tunnel Velocimetry Results for the 1303 UCAV Configuration, AIAA-2006-2990, Jun. 2006.

[3] Ghee T.A and Hall D.R. Experimental and numerical investigation of vortex shedding of a representative UCAV configuration for vortex flow control, *Proc. RTO AVT Symposium on Advanced Flow Management: Part A- Vortex Flows and High Angle of Attack Military Vehicles,* Loer, Norway, RTO-MP-069(I), May 2001.

[4] McParlin S.C, Bruce R.J, Hepworth A.G and Rae A.J. Low speed wind tunnel tests on the 1303 UCAV concept, AIAA 2006-2985, Jun. 2006.

[5] Petterson K. CFD analysis of the low-speed aerodynamic characteristics of a UCAV, AIAA 2006-1259, Jan. 2006.

[6] Wong D.W., McKenzie G.J. , Ol M.V., Petterson, K, and Zhang, S. Joint TTCP CFD Studies into the 1303 UCAV Performance, AIAA 2006-2984, Jun. 2006.

[7] Chung J.J. and Ghee T. Numerical Investigation of UCAV 1303 Configuration with and without Simple Deployable Vortex Flaps, AIAA-2006-2989, Jun. 2006.

[8] Gursul I. Gordnier R and Visbal M. Unsteady aerodynamics of non-slender delta wings, *Progress in Aerospace Sciences*, 2005, **41**, pp. 515-557.

[9] Yaniktepe B and Rockwell D. Flow structure on a delta wing of low sweep angle, *AIAA J,* March 2004, **3,** pp. 513-523.

[10] Taylor G.S. Schnorbus T and Gursul I. An investigation of vortex flows over low sweep delta wings, AIAA 2003-4021, Jun. 2003.

[11] McLain B.K. *Steady and unsteady aerodynamic flow studies over a 1303 UCAV configuration.*MS Thesis, US Naval Postgraduate School, Sep. 2009.

[12] Chua W.H. *Flow visualization studies over a UCAV 1303 model.* M.S. Thesis, Naval Postgraduate School, 2009.

[13] Sosebee P.D. *Flow visualization and detailed load measurements over a maneuvering UCAV 1303.* M.S. Thesis, Naval Postgraduate School, 2011.

[14] Chandrasekhara M.S. and McLain B.K. Aerodynamic studies over a maneuvering UCAV 1303 configuration. To appear, *Aeronautical Journal.*

[15] Medford C.M. The aerodynamics of a maneuvering UCAV 1303 aircraft model and its control through leading edge curvature, M.S. Thesis, Naval Postgraduate School, Sep. 2012.